SCIENCE CHINA
Life Sciences

COVER ARTICLE
•RESEARCH PAPER•

https://doi.org/10.1007/s11427-021-1993-6

Linking circular intronic RNA degradation and function in transcription by RNase H1

Xiang Li[1,2], Jia-Lin Zhang[1,3], Yun-Ni Lei[3,4], Xiao-Qi Liu[2], Wei Xue[3], Yang Zhang[2,#], Fan Nan[3], Xiang Gao[2,4], Jun Zhang[2], Jia Wei[3], Li Yang[3,4] & Ling-Ling Chen[1,2,4*]

[1]*School of Life Science, Hangzhou Institute for Advanced Study, University of Chinese Academy of Sciences, Hangzhou 310024, China;*
[2]*State Key Laboratory of Molecular Biology, Shanghai Key Laboratory of Molecular Andrology, CAS Center for Excellence in Molecular Cell Science, Shanghai Institute of Biochemistry and Cell Biology, University of Chinese Academy of Sciences, Chinese Academy of Sciences, Shanghai 200031, China;*
[3]*CAS Key Laboratory of Computational Biology, Shanghai Institute of Nutrition and Health, Shanghai Institutes for Biological Sciences, University of Chinese Academy of Sciences, Chinese Academy of Sciences, Shanghai 200031, China;*
[4]*School of Life Science and Technology, ShanghaiTech University, Shanghai 201210, China;*
[#]*Current address: Section on Integrative Physiology and Metabolism, Joslin Diabetes Center, Harvard Medical School, Boston, MA 02115, USA*

Received August 14, 2021; accepted August 15, 2021; published online August 25, 2021

Circular intronic RNAs (ciRNAs) escaping from DBR1 debranching of intron lariats are co-transcriptionally produced from pre-mRNA splicing, but their turnover and mechanism of action have remained elusive. We report that RNase H1 degrades a subgroup of ciRNAs in human cells. Many ciRNAs contain high GC% and tend to form DNA:RNA hybrids (R-loops) for RNase H1 cleavage, a process that appears to promote Pol II transcriptional elongation at ciRNA-producing loci. One ciRNA, *ci-ankrd52*, shows a stronger ability of R-loop formation than that of its cognate pre-mRNA by maintaining a locally open RNA structure *in vitro*. This allows the release of pre-mRNA from R-loops by *ci-ankrd52* replacement and subsequent ciRNA removal via RNase H1 for efficient transcriptional elongation. We propose that such an R-loop dependent ciRNA degradation likely represents a mechanism that on one hand limits ciRNA accumulation by recruiting RNase H1 and on the other hand resolves R-loops for transcriptional elongation at some GC-rich ciRNA-producing loci.

circular intronic RNA, ciRNA, *ci-ankrd52*, ciRNA structure, DNA:RNA hybrid, R-loop, RNase H1, transcriptional elongation

Citation: Li, X., Zhang, J.L., Lei, Y.N., Liu, X.Q., Xue, W., Zhang, Y., Nan, F., Gao, X., Zhang, J., Wei, J., et al. (2021). Linking circular intronic RNA degradation and function in transcription by RNase H1. Sci China Life Sci 64, https://doi.org/10.1007/s11427-021-1993-6

INTRODUCTION

Circular intronic RNAs (ciRNAs) are covalently closed noncoding transcripts that accumulate from intron lariats due to the failure of DBR1 debranching (Zhang et al., 2013). The biogenesis of ciRNAs is distinct from that of another type of circular RNAs (circRNAs), which are produced from back-splicing of exon(s) and have been widely studied (Li et al., 2018; Wilusz, 2018; Chen, 2020). So far, the metabolism and functions of ciRNAs have remained largely elusive in cells.

In higher eukaryotic cells, the majority of intron lariats are instantly removed within a few minutes by DBR1 debranching during transcriptional co-splicing (Hesselberth, 2013; Mohanta and Chakrabarti, 2020). A fraction of them remain stable in human cells owing to consensus elements containing a 7 nt GU-rich element near the 5′ splice site and

*Corresponding author (email: linglingchen@sibcb.ac.cn)

an 11 nt C-rich element close to the branchpoint site that protect ciRNAs from DBR1 debranching. Such ciRNAs were found to be partially localized to their sites of transcription and promote parental gene expression *in cis* by an unknown mechanism (Zhang et al., 2013). In addition, stable intronic sequence RNAs (sisRNAs) were found as linear forms in yeast (Morgan et al., 2019) and in *Drosophila melanogaster* (Pek et al., 2015), and as circular forms in *Xenopus oocytes* (Gardner et al., 2012) and in vertebrate cells (Talhouarne and Gall, 2018). ciRNAs are expected to be stable due to their inaccessibility to the linear RNA decay machinery; however, certain turnover mechanism(s) must be involved in ciRNA degradation to prevent their endless accumulation during coupling with Pol II transcription and pre-mRNA splicing.

R-loops are three-stranded structures that harbor a DNA:RNA hybrid and a single stranded DNA, which can interfere with DNA replication, repair and transcription, thus compromising genome integrity and function (Niehrs and Luke, 2020; García-Muse and Aguilera, 2019). In principle, all transcription has the potential to form R-loop structures spontaneously. But cells have taken multiple measures to prevent their formation either by pre-mRNA package (Bonnet et al., 2017) or rapid RNA processing (Li and Manley, 2005) to sequester nascent transcript away from the DNA template. Even so, R-loops can be co-transcriptionally formed mainly in GC-rich sequences, CpG islands, or transcription start or termination sites with GC-skew (Chan et al., 2014; Chen et al., 2017; Ginno et al., 2012). Consequently, different mechanisms and factors are evolved to resolve these R-loops and avoid their accumulation in cells. The most relevant and well-known factor is the endonuclease, RNase H1, which specifically degrades the RNA moiety of DNA:RNA hybrids (Cerritelli and Crouch, 2009; Tadokoro and Kanaya, 2009). However, such RNase H1 cleavage is theoretically costly as it could lead to degradation of nascent precursor mRNAs (pre-mRNAs). Other factors involved in R-loop removal are DNA-RNA helicases, such as DDX5 and DHX9 that can unwind the hybrids (Mersaoui et al., 2019; Cristini et al., 2018) although their modes of action and roles *in vivo* await to be studied in detail. Recent studies also revealed that long noncoding RNAs (lncRNAs) frequently form R-loop structures and regulate gene expression subsequently in mammalian cells. For example, formation of R-loops at target gene promoters (i.e., *Khps1* (Postepska-Igielska et al., 2015) and *APOLO* (Ariel et al., 2020)) modulates gene transcription. Further, back-spliced circRNAs, *circSEP3* and *circSMARCA5*, form DNA:RNA hybrids with its template DNA in the gene body, leading to alternative splicing of cognate mRNA in plants (Conn et al., 2017) and in breast cancer cells (Xu et al., 2020), respectively.

Here, via a small-scale screening of endonucleases that can potentially digest ciRNAs, we unexpectedly observed that ciRNAs were degraded by RNase H1. It turned out that a subgroup of ciRNAs form DNA:RNA hybrids at their producing loci in human cells and that RNase H1 cleaves such ciRNAs in an R-loop dependent manner. We found that *ci-ankrd52* maintained a more open RNA structure than the pre-mRNA and outcompeted the pre-mRNA in forming stable R-loops *in vitro*. The ciRNA in the R-loop was subsequently removed by RNase H1 cleavage. Together, such an unexpected RNase H1-mediated ciRNA degradation via R-loop formation likely provides a mechanism to resolve R-loops formed during Pol II transcriptional elongation without sacrificing nascent pre-mRNAs.

RESULTS

ciRNAs are cleaved by RNase H1 in human cells

ciRNAs, having survived from DBR1 debranching, exist in a covalently closed conformation with a 2′,5′ phosphodiester bond in cells. As they are continuously produced co-transcriptionally from pre-mRNAs, we wondered whether any endonuclease might be responsible for their degradation to prevent excessive accumulation in cells. By screening endonucleases via shRNA-mediated knockdown (KD) in PA1 cells on one abundant ciRNA *ci-ankrd52* (Zhang et al., 2013), we consistently observed increased *ci-ankrd52* accumulation upon RNase H1 loss (Figure 1A; Figure S1A in Supporting Information). As controls, depletion of other endonucleases, such as RNase H2A, showed no effect on *ci-ankrd52* levels (Figure 1A; Figure S1A in Supporting Information). To further confirm this observation, we included another independent shRNA to deplete RNase H1 in PA1 cells and consistent results were obtained (Figure 1B). To exclude potential indirect effects resulted from long-term depletion of RNase H1, we transiently knocked down RNase H1 for 2 days in PA1 cells, and found that *ci-ankrd52* was still obviously accumulated (Figure S1B in Supporting Information). In addition, KD of RNase H1 also led to accumulation of *ci-ankrd52* in 293FT cells (Figure S1C in Supporting Information). These results suggest that RNase H1 degrades *ci-ankrd52* in examined cells.

Besides *ci-ankrd52*, we also examined the effect of RNase H1 on global ciRNA expression in PA1 cells. Total RNAs collected from the scramble shRNA or RNase H1 shRNA-mediated stable KD cells were subjected to RNA-seq after depletion of ribosomal RNAs (Figure S1D in Supporting Information). To identify ciRNAs from RNA-seq with high confidence, we modified the CIRCexpolorer2, which has been widely used for circRNA annotation (Zhang et al., 2016a), for ciRNA annotation by identifying RNA-seq reads mapping to branchpoint sites (CIRCexpolorer-IL; see

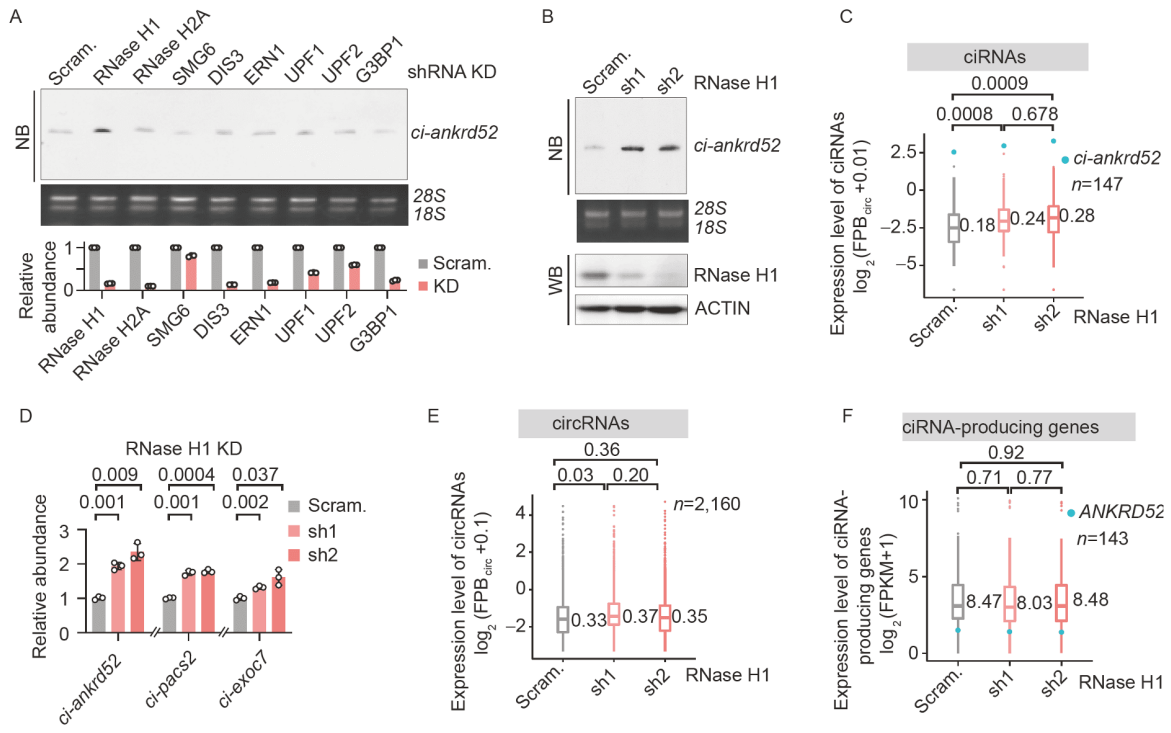

Figure 1 ciRNAs are cleaved by RNase H1 genome-wide. A, Screen of endonucleases identified that RNase H1 degraded *ci-ankrd52*. Top: Northern blot (NB) showed increased *ci-ankrd52* level upon RNase H1 KD in PA1 cells. Middle: rRNAs were used as controls. Bottom: qRT-PCR showed the KD efficiency of different endonucleases by shRNAs. B, Knockdown of RNase H1 by two different shRNAs led to increased *ci-ankrd52* level. Top: NB showed increased *ci-ankrd52* expression upon RNase H1 KD in PA1 cells. Middle: rRNAs were used as controls. Bottom: Western Blot (WB) showed the KD efficiency of RNase H1 by two shRNAs. C, RNase H1 KD led to increased ciRNA expression genome-wide in PA1 cells. High confidence ciRNAs were selected for analysis by FPBcirc ≥0.2 in at least one sample. *ci-ankrd52* was highlighted in blue. The median, IQR, 1.5×IQR and *P* values by Wilcoxon rank-sum test are shown. D, RNase H1 KD led to increased ciRNA expression in PA1 cells, shown by qRT-PCR. The *P* values by Student's *t* test are shown. E, The expression level of back-spliced circRNAs remained unchanged upon RNase H1 KD. High confidence circRNAs were selected for analysis by FPBcirc ≥0.5 in at least one sample. The median, IQR, 1.5×IQR and *P* values by Wilcoxon rank-sum test are shown. F, The expression level of ciRNA-producing genes remained unchanged upon RNase H1 KD. Genes with high confidence ciRNA production in (C) were selected for analysis. *ANKRD52* gene was highlighted in blue. The median, IQR, 1.5×IQR and *P* values by Wilcoxon rank-sum test are shown. See also Figure S1 in Supporting Information.

Methods for details) (Figure S1E in Supporting Information). Totally 3,704 ciRNAs were identified with 147 highly expressed ciRNAs (FPBcirc ≥0.2) in PA1 cells (Figure 1C; Figure S1F in Supporting Information). Genome-wide analyses revealed that depletion of RNase H1 led to increased accumulation of both total and highly-expressed ciRNAs (Figures 1C; Figure S1F and Table S1 in Supporting Information), with about 50% of them upregulated more than 1.5-fold (Figure S1G in Supporting Information). The increased expression of ciRNAs could be verified by qRT-PCR in two independent RNase H1 KD conditions using divergent primers crossing the branchpoint sites featured in ciRNAs (Figure 1D). As controls, the level of back-spliced circRNAs in general remained unchanged upon RNase H1 depletion (Figure 1E); further, the expression level of ciRNA-producing genes also remained largely unchanged (Figures 1F; Figure S1H and Table S1 in Supporting Information), excluding the possibility that RNase H1 may regulate ciRNA levels by affecting their parental gene transcription. These results together suggest that RNase H1 specifically cleaves a subgroup of ciRNAs.

RNase H1 cleaves ciRNAs that form DNA:RNA hybrids at their expression loci

It is intriguing to identify RNase H1 that is responsible for ciRNA turnover, as it is a well-known endonuclease that degrades the RNA strand of DNA:RNA hybrids (Cerritelli and Crouch, 2009). Given the fact of ciRNA localization *in cis* (Zhang et al., 2013), we speculated that ciRNAs could form DNA:RNA hybrids with their DNA templates, and subsequently be cleaved by RNase H1.

Consistent with this notion, introns with ciRNA production (ciRNA introns) have a higher GC%, which is one of features of loci with R-loop formation (Chan et al., 2014; Chen et al., 2017), than that of randomly selected introns without the ability to produce ciRNAs (non-ciRNA introns) (Figures 2A; Figure S2A in Supporting Information). To further test this notion, we evaluated the genome-wide R-loop distribution in PA1 cells using the DNA:RNA hybrid immunoprecipitation (DRIP) assay with the S9.6 antibody that can enrich DNA in DNA:RNA hybrids for DNA sequencing (Figure S2B in Supporting Information). As con-

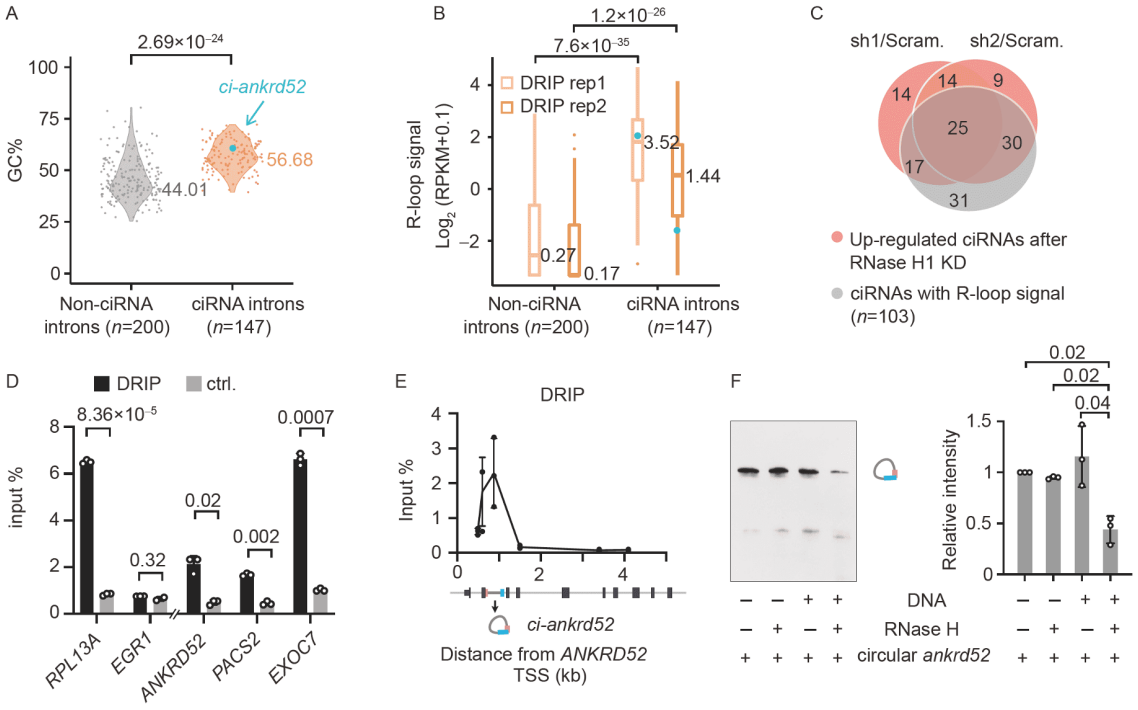

Figure 2 RNase H1 cleaves ciRNAs that form R-loops with template DNA. A, Introns with ciRNA production (ciRNA introns) have a higher GC% than that of introns without ciRNA production (non-ciRNA introns). One hundred and forty-seven ciRNA introns from high confidence ciRNAs in Figure 1D, and 200 randomly selected non-ciRNA introns were analyzed for GC%. *ci-ankrd52* was highlighted in blue. The median, IQR, 1.5×IQR and *P* value by Wilcoxon rank-sum test are shown. B, ciRNA introns contain higher R-loop signals than that of non-ciRNA introns, revealed by DRIP-seq. One hundred and forty-seven ciRNA introns and 200 randomly selected non-ciRNA introns were analyzed for R-loop signals. *ci-ankrd52* intron was highlighted in blue. The median, IQR, 1.5×IQR and *P* value by Wilcoxon rank-sum test are shown. C, The majority of upregulated ciRNAs upon RNase H1 KD display R-loop signals in DRIP-seq results. Upregulated ciRNAs (fold change ≥1.5) in Figure S1F in Supporting Information were used in the analysis. D, Validation of R-loop signals in ciRNA-producing introns in DRIP assays. Three ciRNA introns from *ANKRD52*, *PACS2* and *EXOC7* were confirmed with R-loop signals. *RPL13A* and *EGR1* were used as positive and negative controls, respectively. E, DRIP assay revealed an R-loop peak at the *ci-ankrd52* producing locus. The abscissa is expressed as the distance to the transcriptional start site (TSS) of *ANKRD52*. F, RNase H1 directly cleaved the synthesized circular *ankrd52* in the presence of the DNA template *in vitro*. Left, a representative image of NB in an *in vitro* cleavage assay. Right, statistics of three independent experiments in the left. Images were quantified by Quantity One. In (D–F), error bars represent standard deviation in three independent experiments. *P* values by Student's *t* test are shown. See also Figure S2 in Supporting Information.

trols, samples were pre-treated with RNase H to eliminate the hybrids in DRIP-seq assays. To identify convincing R-loop signals from DRIP-seq data, we quantified the signals by the Reads Per Kilobase per Million mapped reads (RPKM) in DRIP-seq samples (Chen et al., 2017), and then normalized by subtracting the RPKM values in the DRIP control samples that might result from non-specific enrichment by the S9.6 antibody (Figure S2C in Supporting Information). Remarkably, ciRNA introns possessed 8–14-fold higher R-loop signals than that of non-ciRNA introns in two DRIP-seq replicates (Figures 2B; Figure S2D in Supporting Information). Among the upregulated ciRNAs overlapped in different shRNA KDs of RNase H1, ~2/3 (25/39) of them have R-loop signals (Figure 2C; Table S2 in Supporting Information), indicating that RNase H1 can cleave a subgroup of ciRNAs in an R-loop dependent manner.

We further carried out independent assays to confirm R-loop formation at specific ciRNA-producing loci. First, additional DRIP assays revealed notable enrichment of R-loops by the S9.6 antibody in several ciRNA-producing loci including *ANKRD52 intron2*, *PACS2 intron10* and *EXOC7 intron15* (Figures 2D; Figure S2E in Supporting Information) whose ciRNAs were also up-regulated upon RNase H1 depletion (Figure 1D). As controls, positive *RPL13A*, but not negative *EGR1* (Sanz and Chédin, 2019), was enriched in DRIP assays (Figure 2D), confirming the efficiency and specificity of the assays. Importantly, a notable R-loop peak was found at the *ci-ankrd52* producing region (Figure 2E). Second, to confirm that RNase H1 can directly cleave *ci-ankrd52*, *in vitro* synthesized circular *ankrd52* (Figure S2F in Supporting Information) was incubated with purified RNase H enzyme with or without the DNA template. As expected, RNase H cleaved circular *ankrd52* only with the appearance of the corresponding DNA template (Figure 2F). Of note, *in vitro* synthesized circular *ankrd52* is ligated by a 3′,5′ phosphodiester bond, but this does not affect the formation of R-loops with the template DNA (see later, Figures 4 and 5). Lastly, we checked the localization of the endogenous RNase H1 by immunofluorescence (IF) and ciRNAs by fluorescence in situ hybridization (FISH). Endogenous

RNase H1 (>90%) were largely localized to the nucleus with only a small fraction localized to mitochondrion in examined PA1 and 293FT cells (Figure S3A and B in Supporting Information). In addition, endogenous ciRNAs, including *ci-ankrd52*, *ci-pacs2* and *ci-exoc7*, were mainly localized in the nucleus and formed a couple of strong accumulation (Figure 3A; Figure S3C in Supporting Information), likely at their sites of transcription (Zhang et al., 2013). Notably, at least a fraction (~30%) of the endogenous ciRNAs were co-localized with RNase H1 (Figure 3A and B; Figure S3C in Supporting Information), supporting the direct association between ciRNAs and RNase H1 in cells. Collectively, these results reveal that a subgroup of ciRNAs can form R-loops at their producing loci and are subjected by RNase H1 cleavage in an R-loop dependent manner.

Correlation between transcriptional elongation and ciRNA production at the gene body R-loop producing locus

The observation that RNase H1 is responsible for ciRNA degradation in an R-loop dependent manner (Figures 1 and 2) implied that DNA:RNA hybrids were formed prior to RNase H1 cleavage of ciRNAs. During transcription, the formation of DNA:RNA hybrids (R-loops) are closely linked to transcription regulation (García-Muse and Aguilera, 2019). For example, formation of R-loops in gene promoters can activate sense and antisense transcription by providing an open chromatin state (Grunseich et al., 2018; Chen et al., 2015; Tan-Wong et al., 2019), whereas R-loops in gene bodies have been thought to restrain Pol II extension speed during elongation (Shivji et al., 2018). As we have previously shown that ciRNAs could somehow promote parental gene expression *in cis* (Zhang et al., 2013), we asked whether ciRNAs produced from gene bodies exert *in cis* regulation via affecting transcriptional elongation in an R-loop dependent manner.

To test this idea, we first examined the relationship between R-loop levels of different genome regions and gene transcriptional elongation rate (TER) according to 4sUDRB-seq datasets in PA1 cells (Zhang et al., 2016b) (Figure S4A in Supporting Information). This analysis revealed that the TER of genes was negatively correlated with the level of R-loops in gene body regions; whereas little correlation was observed in the promoter or the terminal regions (Figure 3C). Importantly, among all 43 genes (Figure S4A in Supporting Information) with reliable TERs and R-loop signals, those with detectable ciRNA production (n=21) exhibited a higher TER than those without detectable ciRNA production (n=22) (Figure 3D).

It is worth noting that as only ~5% genes could be calculated with TER according to 4sUDRB-seq datasets (Zhang et al., 2016b) and ~1% gene bodies contained R-loop signals ≥2, here we unbiasedly captured 43 genes with both reliable TERs and R-loop signals for analysis. Nonetheless, the R-loop levels of these two groups of genes within their gene body regions were comparable (Table S3 in Supporting Information), and the major difference between these two groups of genes was with or without ciRNA production, indicating that a subgroup of ciRNAs produced from the pre-mRNAs could somehow release the restraint of R-loops on transcriptional elongation.

To support this view, KD of RNase H1 with two different shRNAs both inhibited TER at *ANKRD52* locus, as shown by the quantitative RT-PCR using different primer sets amplified nascent pre-mRNAs (Figure 3E and F), indicating a role of R-loops on transcriptional elongation. Further quantification of the copy number of *ci-ankrd52* by Northern blot showed ~36 copies per PA1 cell (Figure S4B and C in Supporting Information). As ~30% of *ci-ankrd52* signals were co-localized with RNase H1 in PA1 cells (Figure 3A and B; Figure S3C in Supporting Information), there were ~11 copies co-localized with RNase H1, presumably at transcription sites (Zhang et al., 2013). These results indicated that such an abundant *ci-ankrd52* would somehow enable ciRNAs to compete with newly produced pre-mRNAs for R-loop formation with the template DNA during transcriptional elongation.

ci-ankrd52 outcompetes its pre-mRNA to form stable R-loops with template DNA

Next, we asked how ciRNAs would promote Pol II transcriptional elongation *in cis* using *ci-ankrd52* as an illustration. As R-loops formed by pre-mRNAs co-transcriptionally would impede transcription elongation (García-Muse and Aguilera, 2019) and DNA-RNA helicases were reported to regulate R-loop formation (Mersaoui et al., 2019; Cristini et al., 2018), one possibility would be that *ci-ankrd52* could recruit such DNA-RNA helicases to resolve these R-loops formed by pre-mRNAs with the template DNA to release Pol II elongation pausing. To test this idea, we first asked what RNA binding proteins (RBPs) could interact with *ci-ankrd52*. Biotin-labeled circular or linear RNAs were synthesized *in vitro* and were subjected to pull-down assays in PA1 cell lysates, followed by mass spectrometry to identify RBPs that interacted with the circular but not the linear *ankrd52* (Figure S5A in Supporting Information). This approach allowed the identification of a group of RBPs that preferred to bind circular *ankrd52* (Table S4 in Supporting Information). Among them, the DEAD-box helicases, DDX5 (Mersaoui et al., 2019) and DDX21 (Song et al., 2017), as well as the RNA helicase DHX9 (Cristini et al., 2018) with reported roles in regulating R-loop metabolism were selected for validation (Figure S5A in Supporting Information). However, knockdown of these factors using corresponding

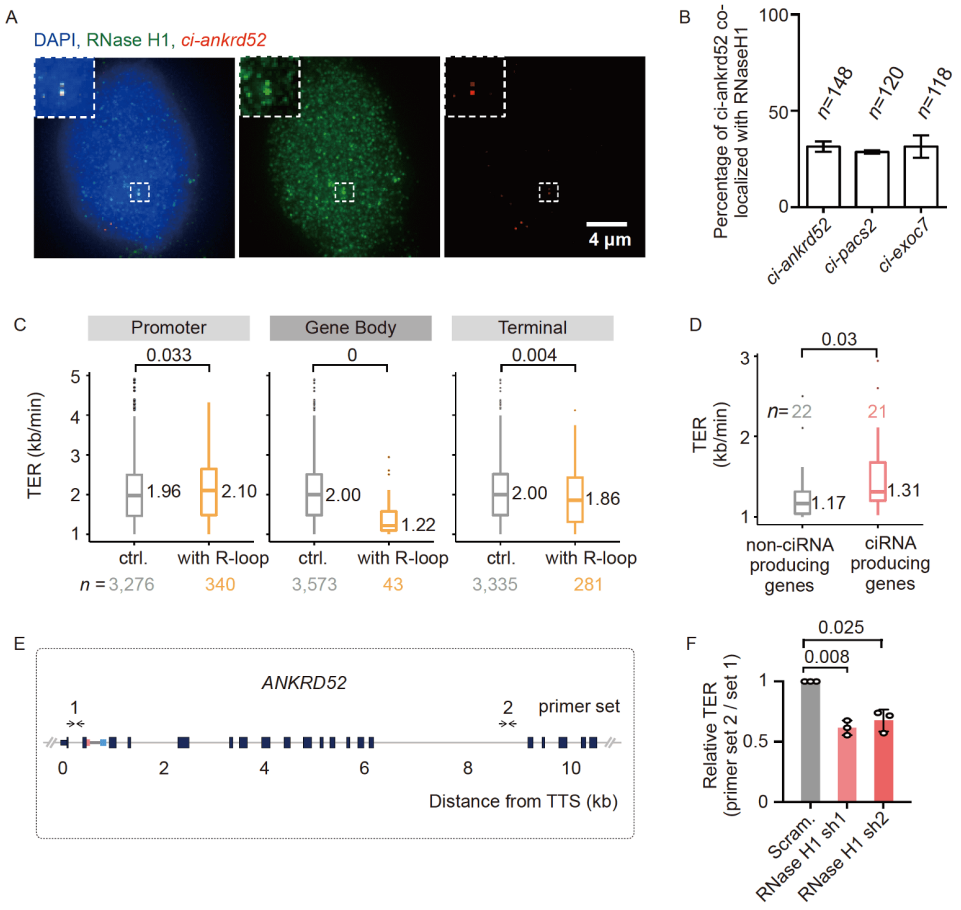

Figure 3 *ci-ankrd52* facilitates transcriptional elongation across its producing locus in an R-loop dependent manner. A, Representative images of immunofluorescence of RNase H1 and fluorescence *in situ* hybridization of *ci-ankrd52* in PA1 cells. DAPI was used as a nuclear marker. B, ciRNAs, including *ci-ankrd52*, *ci-pacs2* and *ci-exoc7*, were partially co-localized with endogenous RNase H1 in PA1 cells. Statistical results were quantified by ImageJ in Figure 3B and Figure S3C in Supporting Information. Data are presented as mean±SD. C, TERs of genes were negatively correlated with the level of R-loops in gene body regions. The numbers of genes with or without R-loop signals in the promoter, gene body and terminal are shown in the bottom and used for TER analysis. All genes that can calculate their TERs were selected, no matter whether these genes could produce ciRNA(s) or not. The median, IQR, 1.5×IQR and *P* values by permutation test are shown. D, Genes with ciRNA production exhibited a higher TER than those without ciRNA production. Forty-three genes with reliable TERs and R-loop signals in gene body regions in (C) were used for analysis. The median, IQR, 1.5×IQR and *P* value by Wilcoxon rank-sum test are shown. E, An illustration of *ANKRD52* organization. The primer sets (F) are shown. F, KD of RNase H1 led to reduced TER across the *ci-ankrd52* producing locus. The distal primer set2 normalized to the proximal primer set1 was used to reflect the TER at this locus under different conditions. Error bars represent standard deviation in three independent experiments. *P* values by Student's *t* test are shown. See also Figures S3 and S4 in Supporting Information.

shRNAs showed little effect on the expression of *ci-ankrd52* or its mRNA (Figure S5B–D in Supporting Information), excluding the possibility that *ci-ankrd52* facilitates Pol II transcription via recruiting these RBPs to resolve R-loops during transcriptional elongation.

Another possibility was that *ci-ankrd52* itself could directly participate in resolving such R-loops formed by pre-mRNAs during transcriptional elongation, by replacing pre-mRNAs to form new R-loops with the template DNA; subsequently, removing *ci-ankrd52* by RNase H1 would resolve the pre-mRNA-formed R-loops to facilitate transcriptional elongation. To test this model, we first compared the ability of *ci-ankrd52* and its cognate linear pre-mRNA to form R-loops *in vitro*. The purified circular or linear *ankrd52* was incubated with its DNA template *in vitro*, followed by R-loop detection with the S9.6 antibody (Figure 4A). We found that both circular and linear *ankrd52* could form R-loops with DNA templates at low hybridization stringency (Figure 4A and B). Remarkably, increasing the hybridization stringency by decreasing ionic strength from 50 to 0.01 mmol L^{-1} led to a sharp reduction of R-loop signals formed by linear *ankrd52*, while those formed by circular *ankrd52* remained more stable (Figure 4A and B). These results suggest that the circular form of *ankrd52* possesses a stronger R-loop formation capability than the linear form.

Next, we designed an *in vitro* R-loop competition assay by adding circular *ankrd52*, linear *ankrd52* or another circular RNA, *circHomer1*, which is produced from back-spliced exon 2–5 of the *HOMER1* gene (You et al., 2015) as different competitors into pre-existing R-loop formation reactions with Dig-labeled linear *ankrd52* (*pre-ANKRD52*), followed by Northern blot of the Dig-labeled linear *ankrd52* after the

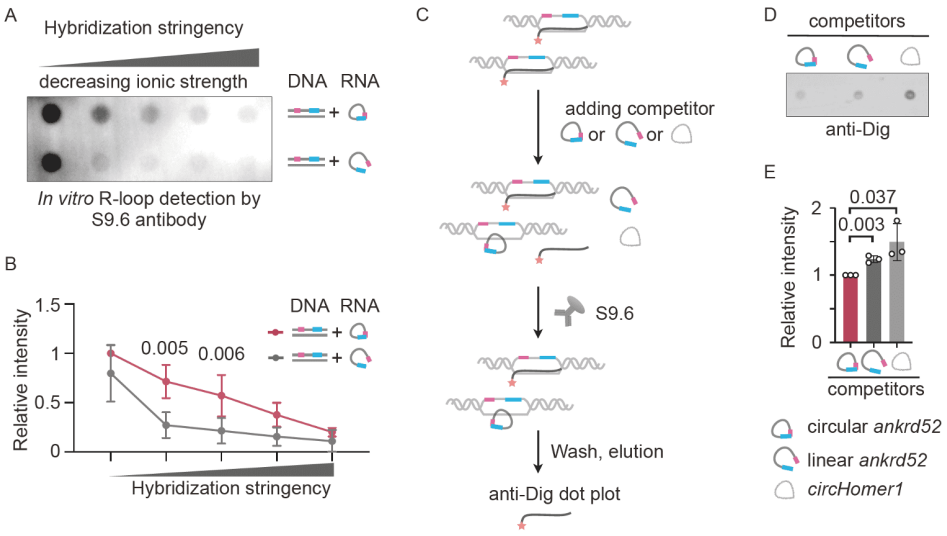

Figure 4 *ci-ankrd52* outcompetes the pre-RNA strand to form a stable DNA:RNA hybrid. A, R-loops formed by circular *ankrd52* are more stable than that formed by linear *ankrd52*, shown by *in vitro* R-loop detection assays. Purified circular or linear *ankrd52* was incubated with the template DNA *in vitro*, and S9.6 antibody was used to detect R-loop formation. Increasing hybridization stringency for R-loop formation was performed by gradient dilution of NaCl concentration from 50 to 0.01 mmol L^{-1}. B, Statistics of results shown in (A). Images were quantified by Quantity One in individual assays. C, Flow chart of an *in vitro* R-loop competition assay. Dig-labeled linear pre-RNAs were incubated with the DNA template to form R-loops aforehand. Indicated competitors were then added to compete with dig-labeled linear pre-RNAs for R-loop formation. Finally, dig-labeled linear pre-RNAs in R-loops were enriched by S9.6 antibody and for detection by NB. D, *In vitro* synthesized circular *ankrd52* showed a stronger capacity of competition with the dig-labeled linear pre-RNA for R-loop formation, compared to the linear *ankrd52* with the same sequences or another circular RNA, *circHomer1*. Representative image of *in vitro* R-loop competition assay is shown. E, Statistics of results shown in (D). Images were quantified by Quantity One in individual assays. In (B) and (E), error bars represent standard deviation in three independent experiments. *P* values by Student's *t* test are shown. See also Figure S5 in Supporting Information.

competition (Figure 4C). Among all three types of competitors, adding the circular *ankrd52* led to the lowest level of Dig-labeled *pre-ANKRD52* RNA retained in R-loops; whereas addition of the nonspecific *circHomer1* resulted in the highest level of Dig-labeled *pre-ANKRD52* RNA in R-loops (Figure 4D and E). These results together suggest that *ci-ankrd52* could replace its pre-mRNA strand from the aforehand R-loops by forming more stable R-loops (Figure 4) that can be targets of RNase H1 cleavage (Figure 1; Figure S1 in Supporting Information).

ci-ankrd52 maintains a locally open secondary structure to form stable R-loops with the template DNA

How do the same sequences between circular and linear *ankrd52* lead to distinct abilities to form R-loops with DNA? We speculated that it could be due to different secondary structures they possess. To test this hypothesis, we performed SHAPE-MaP (selective 2′-hydroxyl acylation analyzed by primer extension and mutational profiling) assays to uncover structural conformations of circular or linear *ankrd52* with or without the complementary DNA template *in vitro* (Figure 5A). To discriminate the circular or the linear *ankrd52*, two sets of divergent primers crossing the branchpoint site for *ci-ankrd52* and multiple sets of convergent primers for the linear *ankrd52* were designed. SHAPE-MaP results showed a higher correlation for *ci-ankrd52* folding status between two biological repeats compared to those of linear *ankrd52* (Figure S6A in Supporting Information), indicating that *ci-ankrd52* is more stable in structure, consistent with the structural characteristic of back-spliced circRNAs in cells (Liu et al., 2019). Strikingly, addition of the DNA template led to a sharp reduction of SHAPE reactivity in *ci-ankrd52* from 212 to 248 nt (Figure 5B, top panel), indicating that a potential DNA:RNA hybrid was formed at this region, thereby preventing the nucleotide labeling by SHAPE regent NAI (2-methylnicotinic acid imidazolide). As controls, there was no obvious difference between SHAPE reactivity of linear *ankrd52* with and without DNA (Figure 5B, bottom panel), consistent with a weaker ability of R-loop formation between the linear *ankrd52* and DNA compared to that of the occasion of circular *ankrd52* (Figure 4). Structural remodeling of circular and linear *ankrd52* based on these experimental SHAPE reactivities revealed that *ci-ankrd52* 212–248 nt preferred to be single stranded (Figure S6B in Supporting Information), while the same region in the linear *ankrd52* tended to form an internal double stranded conformation (Figure S6C in Supporting Information), leading to reluctant R-loop formation with the complementary DNA template (Figure 4). Importantly, further deletion or mutation of these critical sequences in *ci-ankrd52* 212–248 nt led to notable reduction of R-loop formation with DNA (Figure 5C and D), supporting the view that *ci-ankrd52* forms a more stable R-loop with the template DNA than the pre-mRNA via a structure-dependent manner.

Collectively, these findings suggest a "replacement and

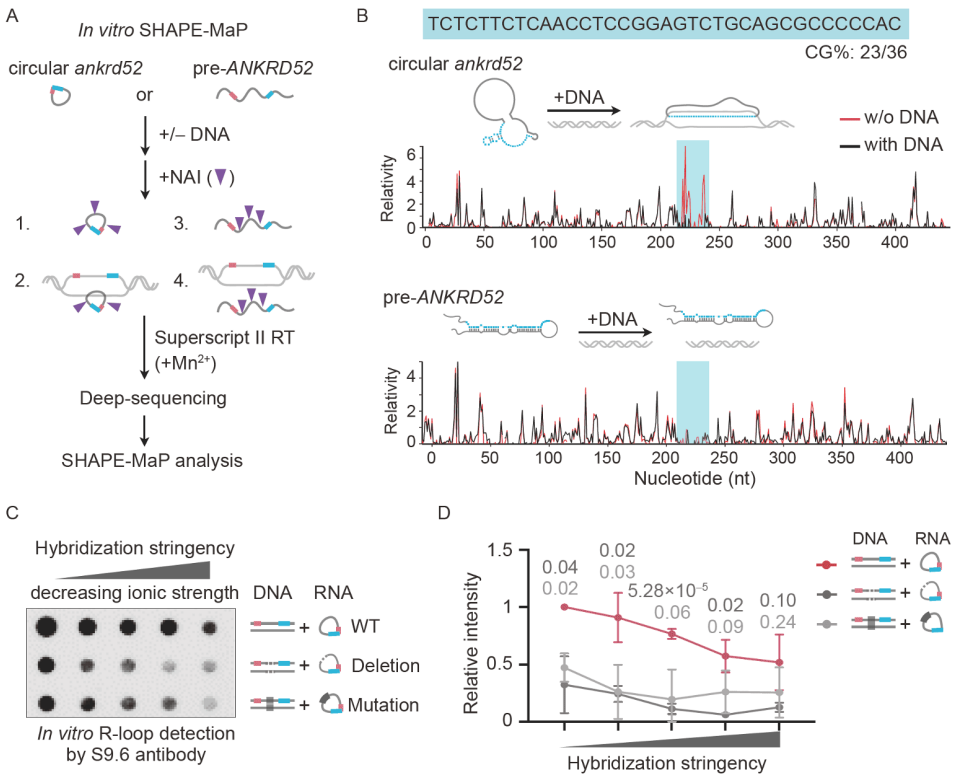

Figure 5 *ci-ankrd52* maintains a locally open RNA structure for preferential R-loop formation. A, An illustration of SHAPE-MaP assays for circular and linear *ankrd52* incubated with or without the DNA template *in vitro*. B, SHAPE-MaP profiles of circular or linear *ankrd52* with or without complementary DNA template. Top, the sequences and GC% of the circular *ankrd52* from 212 to 248 nt. Middle, an illustration of circular *ankrd52* structure and SHAPE-MaP profiles before and after the addition of the DNA template are shown. Bottom, an illustration of linear *ankrd52* structure and SHAPE-MaP profiles before and after the addition of the DNA template are shown. The RNA region (from 212 to 248 nt) is highlighted in blue. C, Deletion or mutation of the sequences in circular *ankrd52* from 212 to 248 nt impaired their R-loop formation capability, shown by *in vitro* R-loop detection assays. D, Quantification of results shown in (C). Images were quantified by Quantity One in individual assays. Error bars represent standard deviation in three independent experiments. *P* values by Student's *t* test are shown. See also Figure S6 in Supporting Information.

cleavage" model that likely occurs in cells, in which the production of *ci-ankrd52* can replace the nascent pre-mRNA in an R-loop within GC-rich gene body region during transcriptional elongation. Further removal of the *ci-ankrd52* by RNase H1 can resolve such pre-mRNA-formed R-loops without sacrificing nascent pre-mRNA levels, facilitating transcriptional elongation *in cis* (Figure 6).

DISCUSSION

R-loops often form during transcription in GC-rich or GC-skew genomic regions, and represent a source of transcriptional elongation pausing, DNA breaks and genome instability (García-Muse and Aguilera, 2019). To avoid these hazards, cells must develop different mechanisms to resolve such harmful R-loops. RNase H1 can cleave the RNA strand in the DNA:RNA hybrids to resolve R-loops (Cerritelli and Crouch, 2009; Tadokoro and Kanaya, 2009); DNA-RNA helicases have been found to unwind the DNA:RNA hybrids to release the RNA strand (Mersaoui et al., 2019; Cristini et al., 2018). Here, we uncovered another possible mechanism to resolve R-loops during transcriptional elongation by a ciRNA that is produced from the same gene. We found that *ci-ankrd52* displayed an open structural conformation that is distinct from pre-mRNA having the same sequences (Figure 5; Figure S6 in Supporting Information). Such altered conformation allowed this ciRNA to replace its pre-mRNA to form more stable R-loops with the template DNA *in vitro* (Figure 4), which likely also occurred at its expression locus (Figures 2 and 3); and subsequently such ciRNA-R-loops were removed by RNase H1-mediated cleavage (Figures 1, 2 and 6). This provides a mechanism to promote transcriptional elongation across the ciRNA-producing gene (Figures 3–5; Figures S3–S6 in Supporting Information). Compared to the canonical way of RNase H1-mediated cleavage of pre-mRNAs to resolve R-loops, the RNase H1-mediated cleavage of ciRNAs is presumably less costly by not sacrificing nascent pre-mRNAs, although the kinetics of the R-loops formed by ciRNAs or pre-mRNAs with the same DNAs in cells remain unknown, due to the lack of appropriate approaches to directly assay the competition between ciRNAs and pre-RNAs for R-loop formation in cells, as well as of tools that can specifically knock down ciRNAs without tar-

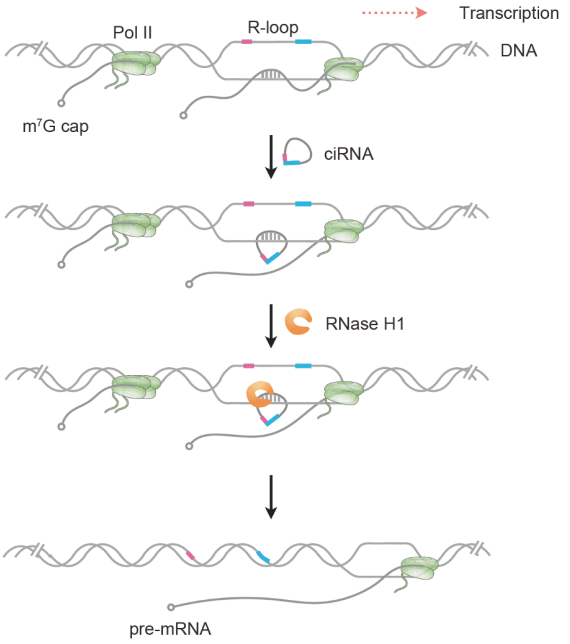

Figure 6 A proposed "replacement and cleavage" model for linking ciRNA degradation and function in resolving R-loops. R-loops formed by pre-mRNA at ciRNA-producing locus with high GC% restrain Pol II elongation speed during transcription. Co-transcriptionally produced ciRNA was proposed to replace the pre-mRNA to form a more stable R-loop at its producing locus. Such a ciRNA-formed R-loop can be further removed by RNase H1 to facilitate the Pol II transcriptional elongation.

geting their cognate pre-RNAs with the same sequences. Nevertheless, given the fact that most ciRNA-producing introns often possess high GC% and R-loop signals (Figure 2; Figure S2 in Supporting Information), such a "replacement and cleavage" model by *ci-ankrd52* and RNase H1 for resolving R-loops (Figure 6) might be applicable to some other ciRNAs (Figures 1D, 3B; Figure S3C in Supporting Information) in cells.

ciRNAs accumulate from intron lariats by escaping from DBR1 debranching during Pol II transcription in human cells (Zhang et al., 2013). How these circular noncoding transcripts are degraded has remained unknown. We unexpectedly identified RNase H1 responsible for ciRNA degradation (Figure 1). Some ciRNAs possess high GC contents and tend to form R-loops allowing subsequent RNase H1 cleavage (Figure 2). Consistent with the notion of forming R-loops *in cis* (Figure 2), ciRNAs have been shown to accumulate at their sites of transcription (Zhang et al., 2013) and partially co-localize with RNase H1 (Figure 3A and B; Figure S3 in Supporting Information). Notably, many lncRNAs form R-loop structures *in cis* (Postepska-Igielska et al., 2015; Ribeiro de Almeida et al., 2018; Ariel et al., 2020), and other types of lncRNAs such as *sno-lncRNA*s (Yin et al., 2012), *SPA*s (Wu et al., 2016) and *JPX* (Tian et al., 2010) were all localized to their transcription sites. It will of interest to explore whether RNase H1 is involved in the turnover regulation of these lncRNAs.

Finally, intron-derived noncoding transcripts have been reported to accumulate and play roles under different pathological conditions. For example, cellular accumulation of RNA lariats caused by DBR1 deficiency resulted in patient susceptibility to severe viral infections of the brainstem (Zhang et al., 2018), suggesting that accumulation of intron lariats is deleterious and needs to be suppressed. Although a fraction of ciRNAs under normal cellular conditions can be cleaved by RNase H1 in an R-loop dependent manner (Figures 1 and 2), and *ci-ankrd52* plays a potential role in resolving R-loops to facilitate transcriptional elongation (Figures 3–5), it is worth noting that such an R-loop-coupled mechanism of ciRNA degradation and R-loop resolving might not act in a predominate way when ciRNAs accumulate abnormally and pathologically. In line with this notion, careful analysis of the available RNA-seq datasets in patient samples (Zhang et al., 2018) did not show a noticeable correlation between the gene expression level and lariat-intron accumulation in patients with DRB1 mutations (data not shown). There are at least two explanations for this observation. First, as only a few copies of ciRNAs are needed to form R-loops *in cis*, additional ciRNA accumulation would unlikely further increase the capability of resolving transcriptionally formed R-loops. Future nascent RNA-seq analyses of patient samples may underscore some correlation between the nascent level of gene expression and stable intron lariat accumulation. Second, besides being localized *in cis* at their transcription sites, ciRNAs or intron lariats can translocate to other sites in the nucleus (Zhang et al., 2013) or even to the cytoplasm (Armakola et al., 2012; Talhouarne and Gall, 2018), indicating additional potential functions *in trans*. Indeed, accumulated intron lariats in the cytoplasm can act as decoys to sequester TDP-43, preventing this protein from interfering with other essential cellular RNAs and RBPs (Armakola et al., 2012). Further, stable intronic transcripts derived from yeast transcriptomes have been shown to regulate growth upon starvation stimulation in a TORC1 pathway dependent manner, which is also not linked to the expression of the host genes (Morgan et al., 2019; Parenteau et al., 2019).

Nonetheless, the proposed model of the R-loop dependent ciRNA degradation is an intriguing mechanism that has the potential to limit circular RNA accumulation by recruiting RNase H1, and to resolve R-loops that impact transcriptional elongation at least at the *ci-ankrd52*-producing locus. Future studies are warranted to examine such a model in other ciRNA-producing loci in both physiological and pathological conditions.

MATERIALS AND METHODS

Experimental model and subject details

Cell lines used in this paper include PA1 (human female

origin), 293FT (human fetus origin) cells. 293FT cells were purchased from ThermoFisher Company, USA (Cat#: R70007). PA1 cells were purchased from the American Type Culture Collection (ATCC; https://www. atcc.org).

E. coli expression strain T1 chemically competent cells were procured from Transgen Biotech, Beijing, China (Cat# CD501-01) and were grown in LB culture at 37°C.

Plasmid constructions

For protein knockdown, DNA sequences for shRNAs that target mRNAs or for a scramble shRNA were individually cloned into pLKO.1-TRC vector.

For *in vitro* R-loop formation and detection assay in Figure 5C and D, DNA sequences from ANKRD52 exon1 to intron3 were amplified from cDNAs of PA1 cells and cloned into the pCDNA3 vector. DNA sequences with indicated mutation or deletion were obtained by overlap PCRs and cloned into the pCDNA3 vector.

All primers for plasmid constructions are listed in Table S5 in Supporting Information. All constructs were confirmed by Sanger sequencing.

Cell culture and cell transfection

PA1, 293FT cells were cultured using standard protocols from ATCC. 293FT cells were maintained in DMEM supplemented with 10% fetal bovine serum (FBS) and 0.1% penicillin/streptomycin. PA1 cells were maintained in MEMα supplemented with 10% FBS, 1% glutamine and 0.1% penicillin/streptomycin. We maintained cell lines at 37°C in a 5% CO_2 cell culture incubator and tested all cell lines routinely for Mycoplasma contamination.

Plasmid transfection was carried out using Lipofectamine 2000 Reagent according to the manufacturer's protocols.

Lentivirus production and cell infection

To produce lentivirus particles, 293FT cells in a 6-cm dish were co-transfected with 5 μg pLKO.1-shRNA constructs or p23-phage constructs, and 3.75 μg psPAX2 and 1.5 μg pMD2.G. The supernatant containing viral particles was harvested twice at 48 and 72 h after transfection, and filtered through Millex-GP Filter Unit (0.22 μm pore size, Millipore). Viral particles were then concentrated about 100-fold by sucrose gradient ultracentrifugation, resuspended in PBS containing 0.1% BSA, and stored at –80°C until use. To infect PA1 cells with lentivirus, cells were incubated with culture medium containing 10 μL concentrated lentivirus and 10 mg mL^{-1} polybrene (Sigma, USA) at 37°C for 24 h. To increase the knockdown efficiency, infected cells were under several days of puromycin selection. Knockdown efficiency of proteins was evaluated by Western blotting (WB).

RNA isolation and qRT-PCR

Total RNAs from cultured cells were extracted with Trizol Reagent (Life Technologies, USA) according to the manufacturer's protocol. RNAs were further treated with DNase I (Ambion, USA; DNA-free kit) and cDNAs were reverse-transcribed with PrimeScript II RTase (TAKARA, Japan) at 42°C for 2 h, and then applied for qPCR analysis using the SYBR Green Realtime PCR Master Mix (TOYOBO, Japan). β-actin mRNA was examined as an internal control for normalization. Expression of each examined target was determined from three independent experiments. Primer sequences for qRT-PCR are listed in Table S5 in Supporting Information.

Protein extraction and Western blotting

Protein samples were collected from cultured cells lysed with 1×SDS loading buffer, and then denatured at 100°C for 10 min. Equal amounts of proteins were separated by electrophoresis on 10% SDS-polyacrylamide gel and transferred to a polyvinylidine difluoride membrane (Millipore , USA). Membrane was then hybridized with indicated primary and secondary antibodies.

Northern blotting

Northern blotting (NB) was performed according to the manufacturer's protocol (DIG Northern Starter Kit, Roche, Switzerland). Digoxigenin (Dig)-labeled antisense riboprobes were made using RiboMAX Large Scale RNA Production Systems (Promega, USA). In brief, 5 μg total RNAs or 1 ng *in vitro* synthesized linear or circular RNAs were resolved on denaturing urea polyacrylamide gel, transferred to nylon membrane (Roche, Switzerland) and UV-cross-linked using standard manufacturer's protocol. Membrane was then hybridized with specific Dig-labeled riboRNA probes. Primers for NB probes are listed in Table S5 in Supporting Information.

Immunofluorescence and fluorescence *in situ* hybridization

Immunofluorescence (IF) and fluorescence *in situ* hybridization (FISH) was carried out as described with slight modifications (Zhang et al., 2013). Briefly, for mitochondria staining, cells were incubated in 50 μmol L^{-1} MitoTracker (Invitrogen , USA) in complete medium for 20 min at 37°C, and the cells were immediately fixed in 4% PFA, 0.4% Glyoxal, 0.1% Methanol. For IF, anti-RNase H1 antibodies (1:200) and fluorescent secondary antibodies were used. For FISH, after IF, cells were subjected to incubation with denatured probes in hybridization buffer (50% formamide in

2×SSC) at 50°C overnight. After hybridization, anti-Dig primary probes and fluorescent secondary antibodies were sequentially added. The nuclei were counterstained with DAPI. Slides were mounted with VECTASHIELD Antifade Mounting Medium (Vector Lab) and imaged on a DeltaVision Elite imaging system (Applied Precision Imaging/GE Healthcare, USA).

In vitro RNA transcription, circularization and purification

In vitro RNA transcription, circularization and purification were performed as described (Liu et al., 2019) with slight modifications. Linear RNAs were *in vitro* transcribed from T7 expression vector prepared by RiboMax large RNA production system (Promega, USA) according to the manufacturer's protocol with slight modifications. Briefly, 1 μg PCR-amplified T7- DNA fragments were incubated with 2 μL T7 RNA polymerase enzyme and 0.5 mmol L^{-1} dNTPs. 2 mmol L^{-1} GMP was supplemented in the reaction to produce 5′-monophosphate RNA that is required for subsequent RNA circularization. *In vitro* transcription was carried out for 2 h at 37°C, followed by DNase I treatment for 30 min at 37°C to remove DNA templates. Transcribed RNAs were precipitated with ethanol, washed with 75% ethanol and resuspended in RNase-free water.

For *in vitro* circularization, 50 μg linear RNAs was incubated with T4 RNA ligase 2 (NEB , USA) in 1 mL reaction for 5 h at 37°C according to the manufacturer's protocol. Circularized or linear RNAs were then concentrated by ethanol precipitation, resolved on denaturing urea polyacrylamide gel and visualized by Ethidium bromide staining. Corresponding bands on denaturing urea polyacryl-amide gel were excised for circular or linear RNA purification. Purified circular or linear RNAs were validated by RNase R treatment as described (Zhang et al., 2014). Primers for circularization are listed in Table S5 in Supporting Information.

Absolute quantification of *ci-ankrd52* copy number

A serial dilutions (0, 10^7, 10^8, 10^9 molecules) of purified circular *ankrd52* and *circCAMSAP1* were added to cell lysates from 1×10^6 PA1 cells for RNA isolation by Trizol regent. *ci-ankrd52* and *circCAMSAP1* were detected respectively by PAGE NB using Dig-labeled riboRNA probes. The copy number of the diluted RNA template was calculated by DNA/RNA Copy Number Calculator from the following website (http://endmemo.com/bio/dnacopynum.php).

Biotinylated RNA pull-down assay

Biotinylated RNA pull down assays were performed as described (Wu et al., 2016) with modifications. *In vitro* synthesized 1 μg biotinylated circular or linear *ankrd52* RNAs was heated for 5 min at 65°C in RNA-folding buffer (10 mmol L^{-1} HEPES and 10 mmol L^{-1} $MgCl_2$) and slowly cooled down to room temperature. Then, 5×10^6 cells were resuspended with 1 mL binding buffer (10 mmol L^{-1} HEPES pH 7.0, 50 mmol L^{-1} KCl, 10% glycerol, 1 mmol L^{-1} EDTA, 1 mmol L^{-1} DTT, 0.5% Triton X-100, heparin 0.3 mg mL^{-1}), sonicated and centrifuged at 13,000 r min^{-1} for 10 min at 4°C. The supernatant was pre-cleared with Streptavidin Dynabeats (Invitrogen, USA) for 30 min at room temperature, followed by incubation with folded RNAs for 30 min and with beads for 10 min. The retrieved proteins were subjected to Western blotting or silver staining for mass spectrum (MS). Silver staining was performed using Pierce Silver Stain for Mass Spectrometry kit (Thermo Fisher Scientific, USA) according to the manufacturer's instructions. After silver staining, specific bands were cut for MS analysis. Identified proteins by MS are listed in Table S4 in Supporting Information.

DNA:RNA hybrid immunoprecipitation (DRIP)

DRIP assay was carried out as described (Ginno et al., 2012) with slight modifications. At least 5×10^6 cultured cells were washed with DPBS, collected and resuspended into 1.6 mL 1×TE buffer (10 mmol L^{-1} Tris pH 8.0, 1 mmol L^{-1} EDTA). Then 83 μL 10% SDS was added to lyse cells at 37°C for 1 h, and 20 μL 20 mg mL^{-1} proteinase K was added to digest proteins at 55°C for at least 10 h. Genomic DNAs (containing RNAs in the hybrid state) were extracted by phenol/chloroform extraction and ethanol precipitation gently. Then the extracted DNAs were fragmented by treatment with restriction enzymes cocktail (*Hin*d III, *Eco*R I, *Bsr*G I, *Xba* I, and *Ssp* I) overnight. Fragmented DNAs were recovered by phenol/chloroform extraction and ethanol precipitation gently, and dissolved into 200 μL water. Half of recovered DNAs were treated with RNase H enzyme (Thermo, USA) to eliminate RNAs in the hybrids overnight at 37°C as DRIP control sample, while the remaining half were treated with water as DRIP sample. Digested DNAs were extracted by phenol/chloroform extraction and ethanol precipitation gently, and dissolved into 100 μL water. 10 μg total DNAs in the DRIP sample or DRIP control sample was used for immunoprecipitation (IP) using 5 μg S9.6 antibody (Karafast, USA) overnight at 4°C, followed by incubation with 50 μL Dynabeads Protein G. The beads were then washed two times with binding buffer (100 mmol L^{-1} $NaPO_4$ pH 7.0, 1.4 mol L^{-1} NaCl, 0.5% Triton X-100) and eluted by elution buffer (50 mmol L^{-1} Tris pH 8.0, 10 mmol L^{-1} EDTA, 0.5% SDS) with Proteinase K at 55°C for 1 h. At last, DNAs in the DNA:RNA hybrids were extracted by phenol/chloroform extraction and ethanol precipitation for qPCR. For DRIP-seq, extracted DNAs were further digested with 0.1 mg mL^{-1}

RNase A at 37°C for 1 h and recovered by phenol/chloroform extraction and ethanol precipitation. Primers are listed in Table S5 in Supporting Information.

Metabolic labeling of nascent RNAs with 4sU and nascent RNA purification

Metabolic labeling of newly transcribed RNAs was performed as described (Zhang et al., 2016b) with modifications. PA1 cells were incubated with 100 mmol L^{-1} DRB for 3 h to block Pol II transcription. Transcription was recovered after DRB removal and newly transcribed RNAs were labeled with 300 mmol L^{-1} 4sU for 10 min. TRizol was added to stop transcription, and total RNAs were extracted. 40 μg 4sU-labeled total RNAs was incubated with 0.2 mg mL^{-1} EZ-link biotin-HPDP (Pierce, USA; 21341, dissolved in dimethylformamide (DMF, Sigma, USA; D4551) at a concentration of 1 mg mL^{-1}) in biotinylation buffer (10 mmol L^{-1} Tris pH 7.4, 1 mmol L^{-1} EDTA) for 1.5 h at room temperature with rotation. Biotinylated RNAs were extracted twice by chloroform to remove unbound biotin-HPDP and precipitated using equal volume of isopropanol and 1:10 volume of 5 mol L^{-1} NaCl. RNAs were precipitated at 13,000 r min^{-1} for 15 min at 4°C, washed twice with 75% ethanol and resuspended in 100 μL RNase-free water. Biotinylated 4sU-labeled RNAs were incubated with 100 mL streptavidin beads (Invitrogen, USA) for 20 min at room temperature. Beads were washed four times with 0.9 mL washing buffer (100 mmol L^{-1} Tris pH 7.4, 10 mmol L^{-1} EDTA, 1 mol L^{-1} NaCl, 0.1% Tween 20, pre-warmed at 65°C), followed by four washes with 0.9 mL washing buffer (at room temperature). Nascent RNAs were eluted twice with 100 μL 0.1 mol L^{-1} dithiotheitol (DTT) and precipitated in 600 μL ice-cold ethanol. The enriched nascent RNAs were used for qRT-PCR with primers listed in Table S5 in Supporting Information.

In vitro R-loop formation and detection assay

Equal amount of *in vitro* synthesized circular or linear *ANKRD52* intron2 sequences were incubated with the DNA template respectively, heated for 5 min at 65°C in hybridization buffer (10 mmol L^{-1} pH 7.5 Tris-HCl, 0.1 mmol L^{-1} EDTA, different NaCl concentration from 50 to 0.01 mmol L^{-1}) and slowly cooled down to room temperature for R-loop formation *in vitro*. Then DNA:RNA hybrids were detected by Dot Blotting analysis using S9.6 monoclonal antibody.

In vitro R-loop competition assay

In vitro synthesized circular and linear *ankrd52*, and *circHomer1* were heated for 5 min at 65°C in PA buffer (10 mmol L^{-1} pH 7.5 Tris-HCl, 0.1 mmol L^{-1} EDTA, 50 mmol L^{-1} NaCl) and slowly cooled down to room temperature as competitors. Meanwhile, 300 pmol purified DNA template and 300 pmol Dig-labeled *in-vitro* synthesized *pre-ANKRD52* were mixed and heated for 5 min at 65°C in PA buffer and slowly cooled down for R-loop formation beforehand. Then, 100 pmol indicated competitor was added and incubated with the pre-existing R-loop formation reactions for 2 h at 37°C. Then the mixture was incubated with 1 μg S9.6 antibody for 2 h at room temperature in 500 μL binding buffer (100 mmol L^{-1} HEPES pH7.0, 50 mmol L^{-1} KCl, 10% glycerol, 1 mmol L^{-1} EDTA, 1 mmol L^{-1} DTT, 0.5% TritonX-100 heparin), followed by incubation with Dynabeads Protein G (Invitrogen, USA) and 20 μg mL^{-1} yeast tRNA for 1 h at room temperature. After washing four times by binding buffer, DNA:RNA hybrids were eluted with elution buffer (100 mmol L^{-1} Tris pH 6.8, 1% SDS, 10 mmol L^{-1} EDTA) for 10 min at 37°C, and used for Dot Blotting analysis using anti-Dig antibody.

In vitro SHAPE-MaP

In vitro synthesized circular or linear *ankrd52* RNAs were incubated with or without an equal amount of DNA template respectively, heated for 5 min at 65°C in PA buffer (10 mmol L^{-1} Tris pH 7.5, 10 mmol L^{-1} $MgCl_2$, 100 mmol L^{-1} NH_4Cl) and slowly cooled down to room temperature *in vitro*. The mixture was then treated with DMSO or SHAPE reagent NAI at a final concentration of 200 mmol L^{-1} respectively and incubated at 37°C for 15 min. Meanwhile, *in vitro* synthesized circular or linear *ankrd52* RNAs were heated for 1 min at 95°C with denaturing buffer (60% formamide, 20 mmol L^{-1} HEPES PH 8.0, 1.6 mmol L^{-1} EDTA PH 8.0), and instantly cooled down to denature RNAs. The denatured RNAs were labeled with NAI at a final concentration of 200 mmol L^{-1} at 95°C for 1 min as denaturing control (DC). RNAs in the reactions were extracted by TRIZOL according to the manufacturer's protocol, followed by DNase I digestion and phenol/chloroform extraction. Next, recovered RNAs were used for reverse transcription using SuperScript II (Invitrogen, USA) and specific primers for circular or linear *ankrd52* RNAs. Finally, nest PCRs were done to amplify circular or linear *ankrd52* DNAs using primers listed in Table S5 in Supporting Information for library preparation and deep sequencing.

Library preparation and deep sequencing

For RNA-seq samples from PA1 cells treated with scram. or RNase H1 shRNAs, ribo minus RNA libraries were prepared using Illumina TruSeq Stranded Total RNA LT Sample Prep Kit according to the manufacturer's protocol with slight modifications in the step for synthesizing first strand cDNA, which used PrimeScript enzyme mix (TAKARA, Japan) for

reverse transcription at 42°C for 2 h.

For SHAPE-MaP RNA-seq samples, libraries were prepared from 1 ng of circular or linear *ANKRD52* DNAs amplified by nest PCR using Illumina TruSeq ChIP Sample Prep Kit.

All libraries were size-selected with AmpureXP beads (Agencourt) and quantified using Agilent Bio analyzer 2100 and Qubit high-sensitivity dsDNA assay. Size-selected libraries were subjected to deep sequencing with Illumina NextSeq 500 (USA) at CAS-MPG Partner Institute for Computational Biology Omics Core, Shanghai, China. Raw read qualities were evaluated by FastQC.

RNA-seq analyses

Deep sequencing datasets were first filtered by using Trimmomatic (Bolger et al., 2014) (version: 0.38; parameters: PE -threads 16 -phred33 TruSeq3- PE-2.fa:2:30:10 LEADING:3 TRAILING:3 SLIDINGWINDOW:4:15 MINLEN:50) to remove low-quality bases and adaptor sequences at both ends of reads. Next, RNA-seq reads were uniquely aligned to rDNA sequences for pre-rRNAs (18S, 5.8S, 28S, and spacer regions) by Bowtie (version: 1.1.2; parameters: -m 1 -k 1 -v 2 -S -p 16) to remove reads mapped to rDNA regions, and then aligned to GRCh38/hg38 human reference genome with the GENCODE gene annotation (v28) by HISAT2 (Kim et al., 2015) (version: 2.1.0; parameters: –no-softclip –rna-strandness RF –score-min L,-16,0 –mp 7,7 –rfg 0,7 –rdg 0,7 –max-seeds 20 -k 10 -t -p 20). HISAT2-unmapped fragments were then mapped to the same GRCh38/hg38 reference genome using TopHat-Fusion (version: 2.0.12; parameters: tophat2 -fusion-search –keep-fasta-order –bowtie1 –no-coverage-search) for subsequent circular intronic RNA (ciRNA) identification and quantification.

Gene expression levels were calculated with FPKM (Fragments Per Kilobase of transcript per Million mapped reads) by StringTie (version: 2.0, parameters: -p 20 -e -G). The maximum FPKM of expressed transcripts of a given gene was selected to represent the expression level of this gene. Expression of genes in PA1 cells with or without RNase H1 KD is listed in Table S1 in Supporting Information.

CircRNA expression was determined by CIRCexplorer-CLEAR as previously reported (Ma et al., 2019). Expression of circRNAs in PA1 cells with or without RNase H1 KD is listed in Table S1 in Supporting Information.

CIRCexplorer-IL for ciRNA annotation

CIRCexplorer-IL was modified from CIRCexporer2 for ciRNA annotation. Briefly, fragments mapped to branch point were retrieved from TopHat-Fusion as previously reported (Zhang et al., 2016a) (parameters: CIRCexplorer2 parse -f -t TopHat-Fusion; CIRCexplorer2 annotate) and which derived from the same intron were annotated as one ciRNA by custom python script (CIRCexplorer-IL). Annotated ciRNAs were quantified by using CIRCexplorer-CLEAR (Ma et al., 2019) (parameter: circ_quant -c -t -l –threshold 20) to obtain FPB (fragments per billion mapped bases) values.

High-confidence ciRNAs were determined with FPBcirc $\geq$0.2 in at least one sample. Identified ciRNAs in PA1 cells with or without RNase H1 KD are listed in Table S1 in Supporting Information. Then, the fold change (FC) of each ciRNA was defined by upregulated (FC $\geq$1.5), unchanged (0.667<FC<1.5) or downregulated (FC $\leq$0.667) one in KD samples, compared to that in control samples in PA1 cells. Meanwhile, the FC of each corresponding linear mRNA was determined in these three types of PA1 cells from KD and controls. All identified ciRNAs and their linear cognate mRNAs are listed in Table S1 in Supporting Information.

GC content calculation

The sequences of ciRNA introns and non-ciRNA introns were extracted. Then custom scripts were used to calculate GC content (GC%) of these regions.

DRIP-seq analyses

DRIP-seq reads were trimmed with Trimmomatic (version: 0.38; parameters: PE -threads 16 -phred33 TruSeq3- PE-2.fa:2:30:10 LEADING:3 TRAILING:3 SLIDINGWINDOW:4:15 MINLEN:50) and mapped to the hg38 (human) using Bowtie2 (Liu and Schmidt, 2012) (version: 2.3.5; default parameters). Duplicated reads were removed by Picard (http://broadinstitute.github.io/picard) (version: 2.22.1; parameters: MarkDuplicates REMOVE_DUPLICATES=true).

For calculating R-loop signal of specific regions, the remaining mapped reads were intersected with the genomic location of these regions (bed format) using BEDTools (Quinlan and Hall, 2010) (version: 2.28.0; parameters: intersect -c -bed) to get the count numbers and further normalized by RPKM (Reads Per Kilobase Million). The averaged RPKM of control samples (with RNase H1 treatment) and DRIP samples were calculated as $Control_{RPKM}$ and $DRIP_{RPKM,}$ respectively. Finally, the R-loop signal value is defined as $DRIP_{RPKM}$ - $Control_{RPKM}$, and R-loop regions should be determined as R-loop signals $\geq$2.

Transcription elongation rate calculation

4sUDRB-seq reads were pre-treated with the pipeline as described above for RNA-seq analyses to get clean reads. Then, these reads were analyzed by using TERate (Zhang et al., 2016b) to evaluate the transcription elongation rate of RNA Pol II for all expressed genes by counting the normalized average hits.

SHAPE reactivity calculation

The SHAPE-MaP results of pre-*ANKRD52* with or without DNA template were analyzed by ShapeMapper software (Busan and Weeks, 2018) (version: 2.1.3; parameters: –verbose –serial –min-depth 1000 –modified –untreated –denatured). SHAPE-MaP results of *ci-ankrd52* with or without DNA template were analyzed by CIRCshapemapper (Liu et al., 2019) with default parameters.

RNA secondary structure modeling

With SHAPE reactivity values determined above, the secondary structures of pre-*ANKRD52* and *ci-ankrd52* with or without DNA template were modeled by RNAfold (Lorenz et al., 2011) (version: 2.4.2, parameters: linear RNAs (deault); circular RNAs (-p -d2 –circ –shape=SHAPE reactivity profile –shapeMethod=D < RNA.fa)).

Statistical analyses

Statistical significance for comparisons of means was generally assessed by Student's *t* test. Statistically significant difference for RNA-seq was assessed by Wilcoxon rank-sum test (R version: 3.6.3). To evaluate the statistical significance between the two groups (with or without R-loop signals) in three genome regions (Figure 3C), permutation test was performed with R platform (R version: 3.6.3).

Accession numbers

All sequencing data reported in this paper are deposited in the GEO (Gene Expression Omnibus) and NODE (National Omics Data Encyclopedia). For RNA-seq in PA1 cells with or without RNase H1 depletion, DRIP-seq in PA1 cells and SHAPE-MAP *in vitro*, the accession number is NODE: OEP002625. For 4sUDRB-seq in PA1 cells, the accession number is GEO: GSE73325.

Contact for reagent and resource sharing

Further information and requests for reagents may be directed to, and will be fulfilled by the corresponding author L.-L. Chen (linglingchen@sibcb.ac.cn).

Compliance and ethics *The author(s) declare that they have no conflict of interest.*

Acknowledgements *We would like to thank Chen and Yang laboratories for discussion, and Qianwen Sun for providing helpful comments on DRIP assays. This work was supported by the National Natural Science Foundation of China (NSFC) (91940303, 31725009) and the HHMI International Program (55008728) to L.-L.C., NSFC (31730111, 31925011) to L.Y. and Young Elite Scientists Sponsorship Program (2020QNRC001) to X.L. L.-L. C. acknowledges the support from the XPLORER PRIZE.*

References

Ariel, F., Lucero, L., Christ, A., Mammarella, M.F., Jegu, T., Veluchamy, A., Mariappan, K., Latrasse, D., Blein, T., Liu, C., et al. (2020). R-loop mediated trans action of the APOLO long noncoding RNA. Mol Cell 77, 1055–1065.e4.

Armakola, M., Higgins, M.J., Figley, M.D., Barmada, S.J., Scarborough, E. A., Diaz, Z., Fang, X., Shorter, J., Krogan, N.J., Finkbeiner, S., et al. (2012). Inhibition of RNA lariat debranching enzyme suppresses TDP-43 toxicity in ALS disease models. Nat Genet 44, 1302–1309.

Bolger, A.M., Lohse, M., and Usadel, B. (2014). Trimmomatic: a flexible trimmer for Illumina sequence data. Bioinformatics 30, 2114–2120.

Bonnet, A., Grosso, A.R., Elkaoutari, A., Coleno, E., Presle, A., Sridhara, S.C., Janbon, G., Géli, V., de Almeida, S.F., and Palancade, B. (2017). Introns protect eukaryotic genomes from transcription-associated genetic instability. Mol Cell 67, 608–621.e6.

Busan, S., and Weeks, K.M. (2018). Accurate detection of chemical modifications in RNA by mutational profiling (MaP) with ShapeMapper 2. RNA 24, 143–148.

Cerritelli, S.M., and Crouch, R.J. (2009). Ribonuclease H: the enzymes in eukaryotes. FEBS J 276, 1494–1505.

Chan, Y.A., Aristizabal, M.J., Lu, P.Y.T., Luo, Z., Hamza, A., Kobor, M.S., Stirling, P.C., and Hieter, P. (2014). Genome-wide profiling of yeast DNA:RNA hybrid prone sites with DRIP-chip. PLoS Genet 10, e1004288.

Chen, L., Chen, J.Y., Zhang, X., Gu, Y., Xiao, R., Shao, C., Tang, P., Qian, H., Luo, D., Li, H., et al. (2017). R-ChIP using inactive RNase H reveals dynamic coupling of R-loops with transcriptional pausing at gene promoters. Mol Cell 68, 745–757.e5.

Chen, L.L. (2020). The expanding regulatory mechanisms and cellular functions of circular RNAs. Nat Rev Mol Cell Biol 21, 475–490.

Chen, P.B., Chen, H.V., Acharya, D., Rando, O.J., and Fazzio, T.G. (2015). R loops regulate promoter-proximal chromatin architecture and cellular differentiation. Nat Struct Mol Biol 22, 999–1007.

Conn, V.M., Hugouvieux, V., Nayak, A., Conos, S.A., Capovilla, G., Cildir, G., Jourdain, A., Tergaonkar, V., Schmid, M., Zubieta, C., et al. (2017). A circRNA from SEPALLATA3 regulates splicing of its cognate mRNA through R-loop formation. Nat Plants 3, 17053.

Cristini, A., Groh, M., Kristiansen, M.S., and Gromak, N. (2018). RNA/DNA hybrid interactome identifies DXH9 as a molecular player in transcriptional termination and R-loop-associated DNA damage. Cell Rep 23, 1891–1905.

García-Muse, T., and Aguilera, A. (2019). R loops: from physiological to pathological roles. Cell 179, 604–618.

Gardner, E.J., Nizami, Z.F., Talbot, C.C., and Gall, J.G. (2012). Stable intronic sequence RNA (sisRNA), a new class of noncoding RNA from the oocyte nucleus of *Xenopus tropicalis*. Genes Dev 26, 2550–2559.

Ginno, P.A., Lott, P.L., Christensen, H.C., Korf, I., and Chédin, F. (2012). R-loop formation is a distinctive characteristic of unmethylated human CpG island promoters. Mol Cell 45, 814–825.

Grunseich, C., Wang, I.X., Watts, J.A., Burdick, J.T., Guber, R.D., Zhu, Z., Bruzel, A., Lanman, T., Chen, K., Schindler, A.B., et al. (2018). Senataxin mutation reveals how R-loops promote transcription by blocking DNA methylation at gene promoters. Mol Cell 69, 426–437.e7.

Hesselberth, J.R. (2013). Lives that introns lead after splicing. WIREs RNA 4, 677–691.

Kim, D., and Salzberg, S.L. (2011). TopHat-Fusion: an algorithm for discovery of novel fusion transcripts. Genome Biol 12, R72.

Kim, G.J., Sock, E., Buchberger, A., Just, W., Denzer, F., Hoepffner, W., German, J., Cole, T., Mann, J., Seguin, J.H., et al. (2015). Copy number variation of two separate regulatory regions upstream of *SOX9* causes isolated 46,XY or 46,XX disorder of sex development. J Med Genet 52, 240–247.

Langmead, B., Trapnell, C., Pop, M., and Salzberg, S.L. (2009). Ultrafast

and memory-efficient alignment of short DNA sequences to the human genome. Genome Biol 10, R25.
Li, H., Handsaker, B., Wysoker, A., Fennell, T., Ruan, J., Homer, N., Marth, G., Abecasis, G., and Durbin, R. (2009). The Sequence Alignment/Map format and SAMtools. Bioinformatics 25, 2078–2079.
Li, X., and Manley, J.L. (2005). Inactivation of the SR protein splicing factor ASF/SF2 results in genomic instability. Cell 122, 365–378.
Li, X., Yang, L., and Chen, L.L. (2018). The biogenesis, functions, and challenges of circular RNAs. Mol Cell 71, 428–442.
Liao, Y., Smyth, G.K., and Shi, W. (2014). featureCounts: an efficient general purpose program for assigning sequence reads to genomic features. Bioinformatics 30, 923–930.
Liu, C.X., Li, X., Nan, F., Jiang, S., Gao, X., Guo, S.K., Xue, W., Cui, Y., Dong, K., Ding, H., et al. (2019). Structure and degradation of circular RNAs regulate PKR activation in innate immunity. Cell 177, 865–880. e21.
Liu, Y., and Schmidt, B. (2012). Long read alignment based on maximal exact match seeds. Bioinformatics 28, i318–i324.
Lorenz, R., Bernhart, S.H., Höner Zu Siederdissen, C., Tafer, H., Flamm, C., Stadler, P.F., and Hofacker, I.L. (2011). ViennaRNA Package 2.0. Algorithms Mol Biol 6, 26.
Ma, X.K., Wang, M.R., Liu, C.X., Dong, R., Carmichael, G.G., Chen, L.L., and Yang, L. (2019). CIRCexplorer3: a CLEAR pipeline for direct comparison of circular and linear RNA expression. Genom Proteom Bioinf 17, 511–521.
Mersaoui, S.Y., Yu, Z., Coulombe, Y., Karam, M., Busatto, F.F., Masson, J. Y., and Richard, S. (2019). Arginine methylation of the ^{DDX}5 helicase $^{RGG/RG}$ motif by ^{PRMT}5 regulates resolution of RNA:DNA hybrids. EMBO J 38, e100986.
Mohanta, A., and Chakrabarti, K. (2020). Dbr1 functions in mRNA processing, intron turnover and human diseases. Biochimie 180, 134–142.
Morgan, J.T., Fink, G.R., and Bartel, D.P. (2019). Excised linear introns regulate growth in yeast. Nature 565, 606–611.
Mortazavi, A., Williams, B.A., McCue, K., Schaeffer, L., and Wold, B. (2008). Mapping and quantifying mammalian transcriptomes by RNA-Seq. Nat Methods 5, 621–628.
Niehrs, C., and Luke, B. (2020). Regulatory R-loops as facilitators of gene expression and genome stability. Nat Rev Mol Cell Biol 21, 167–178.
Parenteau, J., Maignon, L., Berthoumieux, M., Catala, M., Gagnon, V., and Abou Elela, S. (2019). Introns are mediators of cell response to starvation. Nature 565, 612–617.
Pek, J.W., Osman, I., Tay, M.L.I., and Zheng, R.T. (2015). Stable intronic sequence RNAs have possible regulatory roles in *Drosophila melanogaster*. J Cell Biol 211, 243–251.
Postepska-Igielska, A., Giwojna, A., Gasri-Plotnitsky, L., Schmitt, N., Dold, A., Ginsberg, D., and Grummt, I. (2015). LncRNA Khps1 regulates expression of the proto-oncogene SPHK1 via triplex-mediated changes in chromatin structure. Mol Cell 60, 626–636.
Quinlan, A.R., and Hall, I.M. (2010). BEDTools: a flexible suite of utilities for comparing genomic features. Bioinformatics 26, 841–842.
Ribeiro de Almeida, C., Dhir, S., Dhir, A., Moghaddam, A.E., Sattentau, Q., Meinhart, A., and Proudfoot, N.J. (2018). RNA helicase DDX1 converts RNA G-quadruplex structures into R-loops to promote IgH class switch recombination. Mol Cell 70, 650–662.e8.
Sanz, L.A., and Chédin, F. (2019). High-resolution, strand-specific R-loop mapping via S9.6-based DNA–RNA immunoprecipitation and high-throughput sequencing. Nat Protoc 14, 1734–1755.
Shivji, M.K.K., Renaudin, X., Williams, Ç.H., and Venkitaraman, A.R. (2018). BRCA2 regulates transcription elongation by RNA polymerase II to prevent R-loop accumulation. Cell Rep 22, 1031–1039.
Song, C., Hotz-Wagenblatt, A., Voit, R., and Grummt, I. (2017). SIRT7 and the DEAD-box helicase DDX21 cooperate to resolve genomic R loops and safeguard genome stability. Genes Dev 31, 1370–1381.
Tadokoro, T., and Kanaya, S. (2009). Ribonuclease H: molecular diversities, substrate binding domains, and catalytic mechanism of the prokaryotic enzymes. FEBS J 276, 1482–1493.
Talhouarne, G.J.S., and Gall, J.G. (2018). Lariat intronic RNAs in the cytoplasm of vertebrate cells. Proc Natl Acad Sci USA 115, E7970–E7977.
Tan-Wong, S.M., Dhir, S., and Proudfoot, N.J. (2019). R-loops promote antisense transcription across the mammalian genome. Mol Cell 76, 600–616.e6.
Tian, D., Sun, S., and Lee, J.T. (2010). The long noncoding RNA, Jpx, is a molecular switch for X chromosome inactivation. Cell 143, 390–403.
Trapnell, C., Williams, B.A., Pertea, G., Mortazavi, A., Kwan, G., van Baren, M.J., Salzberg, S.L., Wold, B.J., and Pachter, L. (2010). Transcript assembly and quantification by RNA-Seq reveals unannotated transcripts and isoform switching during cell differentiation. Nat Biotechnol 28, 511–515.
Wilusz, J.E. (2018). A 360° view of circular RNAs: from biogenesis to functions. WIREs RNA 9, e1478.
Wu, H., Yin, Q.F., Luo, Z., Yao, R.W., Zheng, C.C., Zhang, J., Xiang, J.F., Yang, L., and Chen, L.L. (2016). Unusual processing generates SPA LncRNAs that sequester multiple RNA binding proteins. Mol Cell 64, 534–548.
Xing, Y.H., Yao, R.W., Zhang, Y., Guo, C.J., Jiang, S., Xu, G., Dong, R., Yang, L., and Chen, L.L. (2017). SLERT regulates DDX21 rings associated with Pol I transcription. Cell 169, 664–678.e16.
Xu, X., Zhang, J., Tian, Y., Gao, Y., Dong, X., Chen, W., Yuan, X., Yin, W., Xu, J., Chen, K., et al. (2020). CircRNA inhibits DNA damage repair by interacting with host gene. Mol Cancer 19, 128.
Yin, Q.F., Yang, L., Zhang, Y., Xiang, J.F., Wu, Y.W., Carmichael, G.G., and Chen, L.L. (2012). Long noncoding RNAs with snoRNA ends. Mol Cell 48, 219–230.
You, X., Vlatkovic, I., Babic, A., Will, T., Epstein, I., Tushev, G., Akbalik, G., Wang, M., Glock, C., Quedenau, C., et al. (2015). Neural circular RNAs are derived from synaptic genes and regulated by development and plasticity. Nat Neurosci 18, 603–610.
Zhang, S.Y., Clark, N.E., Freije, C.A., Pauwels, E., Taggart, A.J., Okada, S., Mandel, H., Garcia, P., Ciancanelli, M.J., Biran, A., et al. (2018). Inborn errors of RNA lariat metabolism in humans with brainstem viral infection. Cell 172, 952–965.e18.
Zhang, X.O., Dong, R., Zhang, Y., Zhang, J.L., Luo, Z., Zhang, J., Chen, L. L., and Yang, L. (2016a). Diverse alternative back-splicing and alternative splicing landscape of circular RNAs. Genome Res 26, 1277–1287.
Zhang, X.O., Wang, H.B., Zhang, Y., Lu, X., Chen, L.L., and Yang, L. (2014). Complementary sequence-mediated exon circularization. Cell 159, 134–147.
Zhang, Y., Xue, W., Li, X., Zhang, J., Chen, S., Zhang, J.L., Yang, L., and Chen, L.L. (2016b). The biogenesis of nascent circular RNAs. Cell Rep 15, 611–624.
Zhang, Y., Zhang, X.O., Chen, T., Xiang, J.F., Yin, Q.F., Xing, Y.H., Zhu, S., Yang, L., and Chen, L.L. (2013). Circular intronic long noncoding RNAs. Mol Cell 51, 792–806.

SUPPORTING INFORMATION

The supporting information is available online at https://doi.org/10.1007/s11427-021-1993-6. The supporting materials are published as submitted, without typesetting or editing. The responsibility for scientific accuracy and content remains entirely with the authors.